Hydrogen Evolution Reaction | Hot Paper

Deutsche Ausgabe: DOI: 10.1002/ange.201507381
Internationale Ausgabe: DOI: 10.1002/anie.201507381

Nanoporous Graphene with Single-Atom Nickel Dopants: An Efficient and Stable Catalyst for Electrochemical Hydrogen Production

H.-J. Qiu, Yoshikazu Ito, Weitao Cong, Yongwen Tan, Pan Liu, Akihiko Hirata, Takeshi Fujita, Zheng Tang, and Mingwei Chen**

Abstract: *Single-atom nickel dopants anchored to three-dimensional nanoporous graphene can be used as catalysts of the hydrogen evolution reaction (HER) in acidic solutions. In contrast to conventional nickel-based catalysts and graphene, this material shows superior HER catalysis with a low overpotential of approximately 50 mV and a Tafel slope of 45 mV dec^{-1} in 0.5 M H_2SO_4 solution, together with excellent cycling stability. Experimental and theoretical investigations suggest that the unusual catalytic performance of this catalyst is due to sp–d orbital charge transfer between the Ni dopants and the surrounding carbon atoms. The resultant local structure with empty C–Ni hybrid orbitals is catalytically active and electrochemically stable.*

Sustainable hydrogen production from electrochemical water splitting by the hydrogen evolution reaction (HER) has attracted growing attention.[1,2] Although platinum-based catalysts can dramatically reduce the overpotential of the HER for fast reaction kinetics, practical implementations of electrochemical hydrogen production have been thwarted by the high costs and the natural scarcity of Pt.[3] The transition metal nickel is known to be a suitable catalyst for the HER in alkaline solutions.[4] Specially, nanostructured Ni alloys with modified electronic structures are excellent HER catalysts in alkaline electrolytes.[5] However, the high catalytic activity of the nickel-based alloys cannot be sustained in acidic solutions because of Ni dissolution, limiting their applications in feasible and operationally simple electrolytic processes that involve the use of proton-exchange membranes. Although great efforts have been devoted to improving the stability of Ni-based catalysts in acidic solutions, for example, by the recent development of Ni_2P nanoparticles[6] and Ni/Mo/N composites,[7] Ni-based catalysts still suffer from low stability and/or insufficient catalytic activity in acidic solutions. Whereas inert graphene itself is not an active HER catalyst, it has recently been demonstrated that nitrogen and sulfur doping can dramatically enhance the catalytic activity of graphene by significantly reducing the overpotential of the HER.[8] In this study, we developed single-atom Ni catalysts anchored to nanoporous graphene (np-G) by incorporating HER-active Ni atoms into chemically stable graphene. The Pt-free single-atom catalysts exhibit superior catalytic activities and exceptional stability in water-splitting reactions in acidic solutions.

Figure 1 a shows a scanning electron microscopy (SEM) image of np-Ni with an atomically thick graphene layer grown by chemical vapor deposition (CVD);[9,10] approximately 100–300 nm large nanopores are uniformly distributed across the sample (Supporting Information, Figure S3 a). Free-standing np-G with doped Ni was chemically exfoliated by dissolving

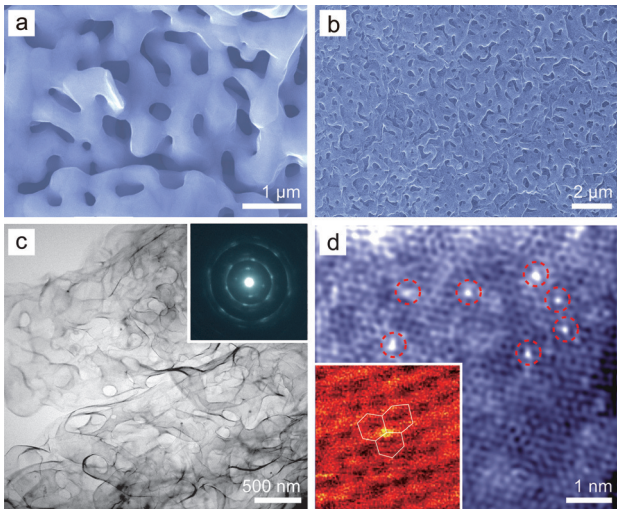

Figure 1. a) SEM image of the as-prepared np-Ni/graphene composite. b) SEM micrograph of Ni-doped np-G after Ni dissolution for six hours. c) TEM image of Ni-doped np-G. Inset: SAED pattern. d) HAADF-STEM image of Ni-doped graphene. Inset: Enlarged HAADF-STEM image (red circle), which shows a substitutional Ni atom (bright orange spot) occupying a carbon site in the graphene lattice (white lines).

[*] Dr. H.-J. Qiu,[+]
School of Chemistry and Chemical Engineering
Chongqing University
Chongqing 400044 (China)
Dr. Y. Ito[+] Dr. Y. Tan, Dr. P. Liu, Dr. A. Hirata, Dr. T. Fujita, Prof. M. Chen
WPI Advanced Institute for Materials Research
Tohoku University
Sendai 980-8577 (Japan)
E-mail: mwchen@wpi-aimr.tohoku.ac.jp
W. Cong,[+] Prof. Z. Tang
State Key Laboratory of Polar Materials and Devices
Ministry of Education of China, East China Normal University
Shanghai 200241 (China)
E-mail: ztang@ee.ecnu.edu.cn
Prof. M. Chen
CREST, Japan Science and Technology Agency
Saitama 332-0012 (Japan)
[+] These authors contributed equally to this work.
Supporting information for this article is available on the WWW under http://dx.doi.org/10.1002/anie.201507381.

the np-Ni templates in 2.0 M HCl solution. After complete np-Ni dissolution, the nanoporous structure of the np-Ni had been inherited by the graphene (Figure 1b). The dissolution of the np-Ni templates with time was investigated by SEM and energy-dispersive X-ray spectroscopy (EDS; Figure S4). A rapid decrease in Ni content was observed at dissolution times of less than five hours; afterwards, the residual Ni concentration decreased only gradually and remained nearly constant after seven hours, indicating that the residual Ni atoms have a strong chemical affinity towards np-G in the samples treated for longer periods of time. EDS analysis confirmed that the Ni content was approximately 4–8 at. % in the sample etched for six hours while the contrast from heavy Ni elements cannot be identified from the SEM image (Figure 1b), indicating the absence of Ni-rich particles. In contrast, the samples that were etched for less than six hours contained Ni particles (Figure S4). The structure of np-G with Ni doping was characterized by transmission electron microscopy (TEM) and scanning TEM (STEM). A bright-field TEM image (Figure 1c) shows the complex 3D morphology of np-G with concave and convex curvatures and nanopores. Except for a small number of dark Ni clusters with sizes of 1–3 nm, Ni nanoparticles were not observed, indicating the full dissolution of the Ni templates. Selected area electron diffraction (SAED; Figure 1c, inset) analysis revealed that the np-G sample had multiple crystallographic orientations, which is associated with the random distribution of the interconnected graphene sheets in the 3D porous structure. Notably, additional diffraction spots from nickel and nickel oxides or hydroxides could not be seen, implying that most Ni dopants in the graphene layer are present as single atoms, rather than as Ni-rich individual phases. A high-resolution TEM (HRTEM) image (Figure S3c) shows that the flat parts of 3D np-G have a perfectly hexagonal structure, the same as for 2D graphene sheets, while topological lattice defects appear in the curved regions to accommodate the large curvature gradients.[10–11] The atomic structure of Ni-doped graphene, imaged by high-angle annular dark field (HAADF) STEM, is shown in Figures 1d and S3d. Aside from a small number of 1–2 nm Ni clusters, single Ni atoms with a bright contrast can be observed, and the number density was determined to be approximately 10^{18}–10^{19} m^{-2}, confirming that most of the residual Ni is present in the form of individual atoms.[12] A zoomed-in image with atomic resolution (Figure 1d, inset) shows that the monoatomic Ni species occupy carbon sites in the graphene lattices. Theoretically, these isolated Ni atoms may be viewed as absorption atoms located in the hollow centers of the six-membered C rings, or as single-atom dopants in substitutional lattice sites or anchored to the lattice defects of graphene (Figure S5). Density functional theory (DFT) calculations show that the binding energies of absorbed, substitutional, and anchored Ni atoms are −0.94 eV, −7.54 eV, and −8.97 eV, respectively. Apparently, substitutional and anchored Ni dopants are energetically favorable because the binding energies are even lower than the cohesive energy of bulk Ni (−4.44 eV).[13]

Ni-doped np-G was further characterized by Raman spectroscopy. As shown in Figure 2a and Table S1, the broad 2D bands (2705 cm^{-1}), together with a low intensity

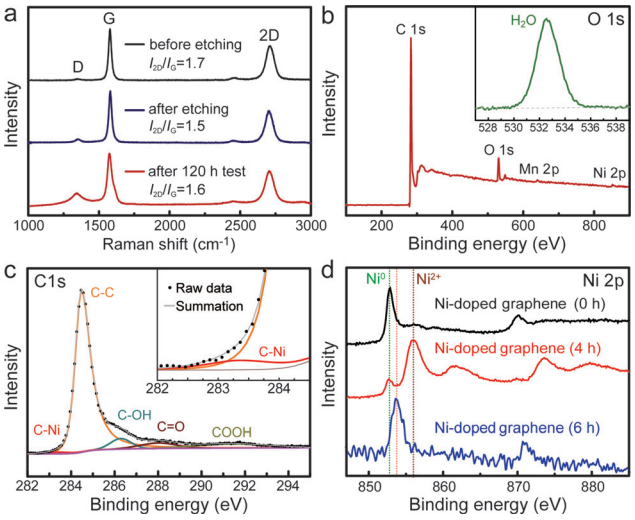

Figure 2. a) Raman spectra of graphene@np-Ni (before etching), substitutional Ni-doped graphene (after etching to dissolve the np-Ni template), and Ni-doped graphene after 120 h HER testing. b) XPS spectrum for all elements in Ni-doped np-G. Inset: Enlarged O 1s spectrum. c) High-resolution C 1s XPS spectrum. Inset: Additional peak towards lower energies resulting from C–Ni bonding. d) High-resolution Ni 2p XPS spectra of pristine graphene@np-Ni (black curve), Ni/np-G with 3 h Ni dissolution (red curve), and Ni-doped graphene with 6 h dissolution (blue curve).

ratio for the 2D and G bands ($I_{2D}/I_G = 1.5$), demonstrate that the 3D nanoporous structure is mainly constructed of bilayer and few-layer graphene. The appearance of weak D bands in the Raman spectra indicates the presence of structural defects,[15] which are geometrically required to coordinate high curvature gradients in 3D nanoporosity.[10–11] The valence state of np-G with Ni doping was determined by X-ray photoelectron spectroscopy (XPS). A Ni-doped np-G sample (6 h dissolution) contained C, O, and Ni as the main elements with a very small amount of residual Mn (Figure 2b). The main peak in the C 1s spectrum (Figure 2c) is located at 284.8 eV and due to graphite-like sp^2-hybridized carbon. A small amount of carbon functional groups, including hydroxy (C–OH), carboxy (COOH), and ketone/aldehyde (C=O) moieties, can be detected.[14] The enlarged C 1s spectrum in Figure 2c, inset shows a slight bump at the low-energy side, indicating a low fraction of C–Ni bonding.[15] The main peak in the O 1s spectrum (Figure 2b, inset) is observed at approximately 533.2 eV, with a shoulder towards higher binding energies. The peak at 533.2 eV is mainly due to H_2O adsorbed on the sample while the shoulder peak may originate from carboxy and hydroxy groups. The binding energy of the Ni $2p_{3/2}$ peak is 853.6 eV (Figure 2d) and thus higher than that reported for Ni^0 (852.5–853.0 eV) and pristine, graphene-coated np-Ni, but similar to that of Ni in nickel carbides.[15] Thus, the Ni $2p_{3/2}$ and C 1s XPS spectra indicate a chemical interaction between the Ni dopants and graphene with possible formation of C–Ni bonding. The peak at about 870.9 eV was assigned to the $2p_{1/2}$ spin–orbit component of zero-valent metallic nickel, suggesting that the atomic Ni residues are in the metallic state and not present as Ni oxides or hydroxides. For comparison, we also

investigated the valence state of Ni in a sample with a short Ni dissolution time of 4 h. In this sample, undissolved Ni was present in the form of nanoparticles (Figure S6). Aside from zero-valent metallic nickel with the Ni $2p_{3/2}$ peak at 852.5 eV and the $2p_{1/2}$ spin–orbit component at 869.7 eV,[15a,16] oxidized Ni with a Ni $2p_{3/2}$ peak at 855.7 eV and a Ni $2p_{1/2}$ peak at 873.4 eV as well as the corresponding shake-up resonances at 861.4 and 880.0 eV was observed (Figure 2d and Figure S6a). The O 1s spectrum shows a main peak at approximately 531.5 eV (Figure S6b), indicating that the oxidized Ni is present in the form of hydroxides. Therefore, the XPS spectrum of Ni in the sample etched for six hours is intrinsically different from those of zero-valent metallic Ni^0 and oxidized Ni, highlighting the unique electronic state of the monoatomic Ni dopants in graphene.

The catalytic performance of the Ni-doped graphene in 0.5 M H_2SO_4 solution was evaluated with a three-electrode setup. As shown in Figures 3a and S7a, samples with short Ni dissolution times (3–5 h) exhibited a high current response owing to the large amount of residual metallic Ni^0. However, an obvious current response was observed between 0 and 0.1 V, which corresponds to the dissolution of excess Ni and hence indicates insufficient electrochemical stability. After Ni dissolution in 2.0 M HCl solution for six hours, the current response between 0 and 0.1 V completely disappeared, indicating that the residual Ni in the form of substitutional dopants has become electrochemically stable. To further test the stability of the samples with different Ni dissolution periods, cyclic voltammetry (CV) experiments between 0.1 and −0.2 V were run for 200 cycles. The electrodes obtained with short Ni dissolution periods of three to five hours showed poor current retention. After Ni dissolution for six hours, the Ni-doped graphene became stable with nearly 100% retention and retained a high electrode current at −0.2 V (Figure S7b). The catalytic performance of the Ni-doped np-G samples (4, 6, and 9 h dissolution) in the HER was compared with Pt and reduced graphene oxide (r-GO) under the same testing conditions. The polarization curve of Ni-doped graphene (6 h dissolution) showed a very low overpotential (η) of approximately 50 mV for the HER (Figure 3a) and a rapid increase in the cathodic current with applied potential. In contrast, r-GO without any Ni dopants exhibited a very low HER activity, which is consistent with a previous report.[17] The HER activity of Ni-doped graphene strongly depends on the concentration of the substitutional Ni dopants. A very low Ni concentration (0.38 at.%; 9 h dissolution) leads to a much lower HER activity (Figure 3a). These results demonstrate that the Ni dopants play a crucial role in determining the HER activity. The overpotential of the Ni-doped graphene catalyst is much lower than or comparable to the best values achieved with Pt-free monolithic catalysts, such as MoS_2 nanosheets (ca. 100–120 mV),[17,18] chemically exfoliated 2D WS_2 (80–100 mV),[19] and metal-free chemically doped graphene (130–290 mV).[8] Moreover, the achieved overpotential is also comparable to those of the best Ni-based catalysts, such as Ni/NiO/$CoSe_2$ in 0.5 M H_2SO_4 solution,[20] but the Ni-doped graphene has a much better stability.

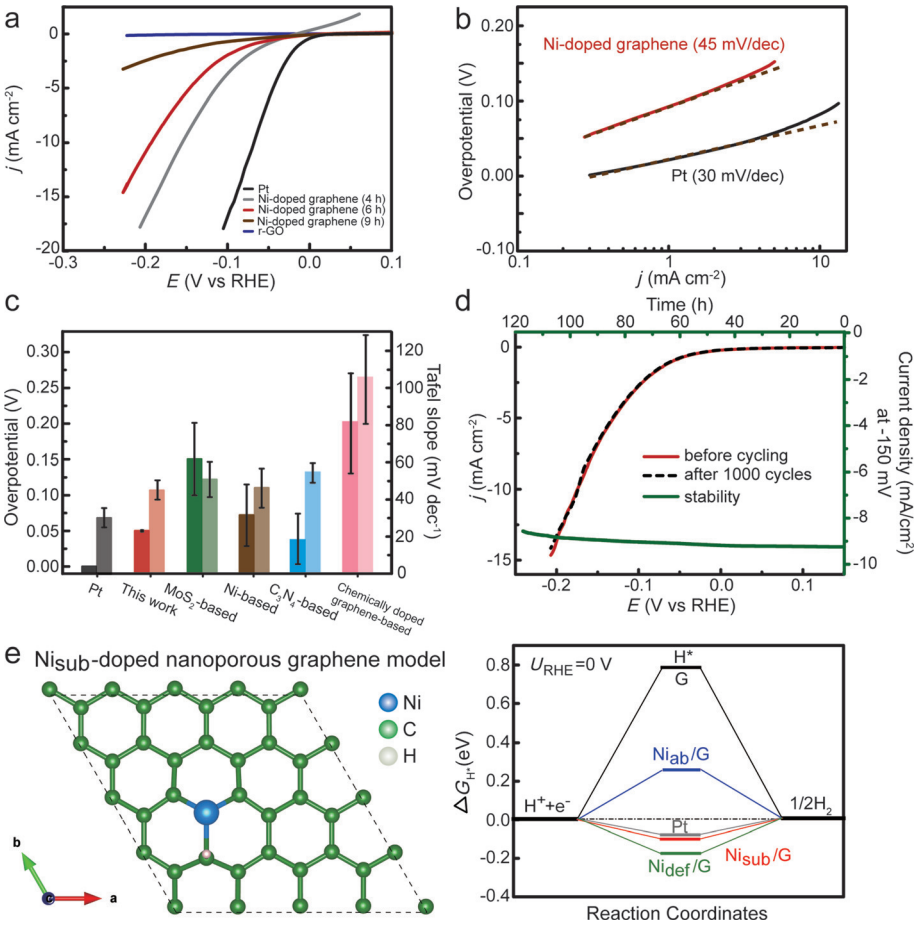

Figure 3. a) Polarization curves of Ni-doped graphene samples with different Ni dissolution periods (4, 6, and 9 h) along with those of Pt and reduced graphene oxide (r-GO) electrodes for comparison. b) Tafel plots of Ni-doped graphene (6 h dissolution) and Pt. c) Overpotential (left) and Tafel slope (right) analysis of different HER catalysts in acid solutions. d) Durability of Ni-doped graphene at a constant overpotential of 150 mV for 120 h (green line) and cycling stability tests (red line: polarization curve of pristine Ni-doped graphene (6 h dissolution); black dashed line: after 1000 cycles). e) Hydrogen adsorption sites and configuration of the Ni_{sub}/G model with $\Delta G_{H^*} = -0.10$ eV (left) and calculated Gibbs free energy diagram (right) of the HER at equilibrium potential for a Pt catalyst and Ni-doped graphene (Ni_{ab}/G, Ni_{sub}/G, and Ni_{def}/G) samples. The free energies for hydrogen adsorption on pristine graphene and Pt metal are plotted for comparison, with $\Delta G_{H^*} = 0.79$ and 0.09 eV, respectively.

The HER kinetics of the Ni-doped graphene were analyzed by Tafel plots. The linear portions of the Tafel plots were fitted to the Tafel equation: $\eta = b\log(j) + a$, where j is the current density, and b is the Tafel slope. The Tafel slope of Ni-doped graphene (6 h dissolution) shows a very low value of about 45 mV dec^{-1} (Figure 3b), which is comparable to the lowest values (41 and 50 mV dec^{-1}) reported for MoS_2-based catalysts.[17–18] A comparison of the Tafel slopes and overpotentials of Ni-doped graphene and previously reported highly efficient HER catalysts is given in Figure 3c and Table S2. Apparently, substitutional Ni doping dramatically changes the chemical activity of graphene from inertness to being one of the best HER catalysts. The intrinsic catalytic activity of Ni-doped np-G was assessed in terms of the exchange current density (j_0), which was calculated from the extrapolated x intercept at $\eta = 0$. The j_0 value of Ni-doped graphene is about 5.3×10^{-2} mA cm^{-2}, which is obviously higher than those of Ni/NiO/$CoSe_2$ (1.4×10^{-2} mA cm^{-2})[20] and MoS_2 based catalysts (5.1×10^{-3} mA cm^{-2}).[21] Based on the number of Ni atoms, the calculated turnover frequency (TOF) is approximately 0.8 s^{-1} at $\eta = 0.3$ V, which is higher than those of most MoS_2-based catalysts (ca. 0.01–0.3 s^{-1}),[3e] demonstrating the high intrinsic catalytic activity of the substitutional monoatomic Ni dopants with a Faradaic efficiency close to 100%.

Electrochemical impedance spectroscopy (EIS) measurements (Figure S7c) show a low internal resistance of 9 ohm (6 ohm cm^{-2}), indicating that the high electrical conductivity of np-G[10] was well retained after Ni doping. At a constant overpotential of 150 mV, Ni-doped graphene showed an excellent HER performance with about 90% retention of the initial activity after running for 120 h (Figure 3d). A Raman spectrum of the cycled sample showed that the long-term testing only led to slight increase in the D band intensity ($I_D/I_G = 0.6$; Figure 2a) in comparison with the as-prepared sample. We also analyzed the cycling stability of Ni-doped np-G under continuous potential scanning. After 1000 cycles, the catalyst only showed negligible cathodic current loss (Figure 3d), and the sample was analyzed by STEM and electron energy loss spectroscopy (EELS; Figure S8). The distribution of the atomic Ni dopants was very similar to that in the as-prepared sample (Figure S3), demonstrating that the single-atomic Ni dopants in np-G are stable under the acidic electrochemical conditions. Separate XPS measurements of the sample after 1000 cycles showed no obvious chemical structure changes of the Ni dopants, further corroborating the high chemical stability of Ni-doped np-G (Figure S9).

The HER reaction mechanism in acidic solutions has been described as a three-stage process consisting of 1) an initial stage of H^+ and e^- generation, 2) an intermediate stage of H* adsorption, and 3) a final stage of $1/2\,H_2$ generation.[17,22] Highly efficient HER catalysts have a Gibbs free energy of H* adsorption, $|\Delta G_{H^*}|$, close to zero;[17,22] this property depends on the geometric and electronic structures of the catalysts. To understand the reasons for the exceptional catalytic activity of single-atomic Ni-doped graphene, we investigated the characteristic structural features and the Gibbs free energy profiles of graphene–Ni catalysts with three possible configurations: The nickel dopants can be present as 1) interstitial atoms in the hollow centers of the benzene rings (Ni_{ab}), 2) substitutional dopants occupying C sites in the graphene lattice (Ni_{sub}), or as 3) anchoring atoms on defect sites (Ni_{def}; Figure S5). The $|\Delta G_{H^*}|$ values of pure graphene and Ni_{ab}-doped graphene (Figure 3e) are positive, indicating that H* cannot be efficiently adsorbed onto the catalysts, and therefore, their catalytic activities are impeded. However, the $|\Delta G_{H^*}|$ values of Ni_{sub}- and Ni_{def}-doped graphene are negative, and in particular, Ni_{sub}-doped graphene has the smallest $|\Delta G_{H^*}|$ value of 0.10 eV, which is similar to those of Pt catalysts ($|\Delta G^{Pt}_{H^*}| \approx 0.09$ eV). For Ni_{def}-doped graphene with different topologic defects (Figure S10), negative Gibbs free energies, ΔG_{H^*}, from −0.40 to −0.26 eV were obtained, which are significantly smaller than that of the Pt catalyst. These results demonstrate that single Ni atoms occupying carbon sites of graphene are the most efficient HER catalysts and therefore play a critical role in the outstanding HER activities.

The exceptional catalytic activity of single-atom catalysts usually arises from unique electronic structures that are due to chemical interactions with the supports.[23] The electronic structure of graphene with Ni_{ab} and Ni_{sub} was investigated with DFT calculations (Figure S11). The Ni_{ab} optimized structure showed that the Ni atoms lie out of the graphene plane by 0.173 nm and revealed an impurity binding energy of only −0.94 eV. The partial density of states (pDOS) projected to the Ni_{ab} atom indicates that the electrons of the impurity occupy nearly degenerate 3d levels, which are just below the Fermi level (E_f) and largely retain the isolated atomic orbital characteristics (Figure S11a). Therefore, the Ni_{ab} atoms are physically adsorbed onto the hollow centers of the graphene surface, and the electronic state of the Ni_{ab}–graphene system is similar to that of pristine graphene with a positive Gibbs free energy of H* adsorption (Figure 3e). However, the Ni_{sub} optimized structure shows that the Ni atom lies out of the graphene plane by only 0.108 nm. The pDOS projected to the Ni atom and the three surrounding C atoms, together with their overlapping (Figure S11b,c), indicates strong C–Ni binding, which is in good agreement with the XPS data. As a result, the binding of the Ni dopant with graphene becomes much more stable with a binding energy of −7.54 eV. In particular, sp–d orbital-charge transfer between the Ni dopant and the surrounding carbon atoms results in an empty C–Ni hybrid orbital close to E_f (Figure S11c), which turns the local structural unit consisting of the Ni dopant and the surrounding C atoms into a catalytically active site because the chemical bond between the H* atom and the hybrid orbital significantly reduces the H* adsorption energy (Figure 3e). Moreover, the chemical bonding that is due to the charge transfer between the Ni dopants and the carbon surrounding apparently stabilizes the Ni species in acidic solutions. Therefore, the interplay between the substitutional monoatomic Ni dopants and the surrounding C atoms leads to exceptional HER catalysis and renders the Ni-doped graphene highly stable.

Acknowledgements

This work was sponsored by JST-CREST ("Phase Interface Science for Highly Efficient Energy Utilization"), JST (Japan), and MEXT. Z.T. was supported by the National Science Foundation of China (61425004, 61227902, and 11175066). H.J.Q. is supported by the JSPS postdoctoral fellowship program (P12054).

Keywords: electrocatalysis · graphene · hydrogen evolution reaction · nanoporosity · nickel doping

How to cite: *Angew. Chem. Int. Ed.* **2015**, *54*, 14031 – 14035
Angew. Chem. **2015**, *127*, 14237 – 14241

[1] a) M. S. Dresselhaus, I. L. Thomas, *Nature* **2001**, *414*, 332 – 337; b) Y. Zheng, Y. Jiao, M. Jaroniec, S. Z. Qiao, *Angew. Chem. Int. Ed.* **2015**, *54*, 52 – 65; *Angew. Chem.* **2015**, *127*, 52 – 66; c) Y. Jiao, Y. Zheng, M. Jaroniec, S. Z. Qiao, *Chem. Soc. Rev.* **2015**, *44*, 2060 – 2086.

[2] M. G. Walter, E. L. Warren, J. R. McKone, S. W. Boettcher, Q. Mi, E. A. Santori, N. S. Lewis, *Chem. Rev.* **2010**, *110*, 6446 – 6473.

[3] a) Y. Zheng, Y. Jiao, Y. Zhu, L. H. Li, Y. Han, Y. Chen, A. Du, M. Jaroniec, S. Z. Qiao, *Nat. Commun.* **2014**, *5*, 3783; b) J. Duan, S. Chen, M. Jaroniec, S. Z. Qiao, *ACS Nano* **2015**, *9*, 931 – 940; c) J. Duan, S. Chen, B. A. Chambers, G. G. Andersson, S. Z. Qiao, *Adv. Mater.* **2015**, *27*, 4234 – 4241; d) S. Chen, J. Duan, Y. Tang, B. Jin, S. Z. Qiao, *Nano Energy* **2015**, *11*, 11 – 18; e) J. D. Benck, T. R. Hellstern, J. Kibsgaard, P. Chakthranont, T. F. Jaramillo, *ACS Catal.* **2014**, *4*, 3957 – 3971; f) E. J. Popczun, C. G. Read, C. W. Roske, N. S. Lewis, R. E. Schaak, *Angew. Chem. Int. Ed.* **2014**, *53*, 5427 – 5430; *Angew. Chem.* **2014**, *126*, 5531 – 5534.

[4] a) Y. Choquette, L. Brossard, A. Lasia, H. Ménard, *Electrochim. Acta* **1990**, *35*, 1251 – 1256; b) N. Danilovic, R. Subbaraman, D. Strmcnik, K. C. Chang, A. P. Paulikas, V. R. Stamenkovic, N. M. Markovic, *Angew. Chem. Int. Ed.* **2012**, *51*, 12495 – 12498; *Angew. Chem.* **2012**, *124*, 12663 – 12666; c) R. Subbaraman, D. Tripkovic, K. C. Chang, D. Strmcnik, A. P. Paulikas, P. Hirunsit, M. Chan, J. Greeley, V. Stamenkovic, N. M. Markovic, *Nat. Mater.* **2012**, *11*, 550 – 557; d) R. Subbaraman, D. Tripkovic, D. Strmcnik, K. C. Chang, M. Uchimura, A. P. Paulikas, V. Stamenkovic, N. M. Markovic, *Science* **2011**, *334*, 1256 – 1260.

[5] a) L. Xiao, S. Zhang, J. Pan, C. X. Yang, M. L. He, L. Zhuang, J. T. Lu, *Energy Environ. Sci.* **2012**, *5*, 7869 – 7871; b) J. R. McKone, B. F. Sadtler, C. A. Werlang, N. S. Lewis, H. B. Gray, *ACS Catal.* **2013**, *3*, 166 – 169; c) F. Rosalbino, S. Delsante, G. Borzone, E. Angelini, *Int. J. Hydrogen Energy* **2008**, *33*, 6696 – 6703; d) N. V. Krstajić, V. D. Jović, L. Gajić-Krstajić, B. M. Jović, A. L. Antozzi, G. N. Martelli, *Int. J. Hydrogen Energy* **2008**, *33*, 3676 – 3687.

[6] a) E. J. Popczun, J. R. McKone, C. G. Read, A. J. Biacchi, A. M. Wiltrout, N. S. Lewis, R. E. Schaak, *J. Am. Chem. Soc.* **2013**, *135*, 9267 – 9270; b) P. C. K. Vesborg, B. Seger, I. Chorkendorff, *J. Phys. Chem. Lett.* **2015**, *6*, 951 – 957.

[7] W. F. Chen, K. Sasaki, C. Ma, A. I. Frenkel, N. Marinkovic, J. T. Muckerman, Y. M. Zhu, R. R. Adzic, *Angew. Chem. Int. Ed.* **2012**, *51*, 6131 – 6135; *Angew. Chem.* **2012**, *124*, 6235 – 6239.

[8] a) Y. Zheng, Y. Jiao, L. H. Li, T. Xing, Y. Chen, M. Jaroniec, S. Z. Qiao, *ACS Nano* **2014**, *8*, 5290 – 5296; b) Y. Ito, W. Cong, T. Fujita, Z. Tang, M. Chen, *Angew. Chem. Int. Ed.* **2015**, *54*, 2131 – 2136; *Angew. Chem.* **2015**, *127*, 2159 – 2164; c) J.-M. Ge, B. Zhang, L.-B. Lv, H.-H. Wang, T.-N. Ye, X. Wei, J. Su, K.-X. Wang, X.-H. Li, J.-S. Chen, *Nano Energy* **2015**, *15*, 567 – 575.

[9] H. J. Qiu, J. L. Kang, P. Liu, A. Hirata, T. Fujita, M. W. Chen, *J. Power Sources* **2014**, *247*, 896 – 905.

[10] a) Y. Ito, Y. Tanabe, H.-J. Qiu, K. Sugawara, S. Heguri, N. H. Tu, K. K. Huynh, T. Fujita, T. Takahashi, K. Tanigaki, M. W. Chen, *Angew. Chem. Int. Ed.* **2014**, *53*, 4822 – 4826; *Angew. Chem.* **2014**, *126*, 4922 – 4926; b) Y. Ito, Y. Tanabe, J. Han, T. Fujita, K. Tanigaki, M. W. Chen, *Adv. Mater.* **2015**, *27*, 4302 – 4307.

[11] Y. Ito, H. J. Qiu, T. Fujita, Y. Tanabe, K. Tanigaki, M. W. Chen, *Adv. Mater.* **2014**, *26*, 4145 – 4150.

[12] H. T. Wang, Q. X. Wang, Y. C. Cheng, K. Li, Y. B. Yao, Q. Zhang, C. Z. Dong, P. Wang, U. Schwingenschlögl, W. Yang, X. X. Zhang, *Nano Lett.* **2012**, *12*, 141 – 144.

[13] G. M. Zhou, D. W. Wang, L. C. Yin, N. Li, F. Li, H. M. Cheng, *ACS Nano* **2012**, *6*, 3214 – 3223.

[14] D. C. Wei, Y. Q. Liu, Y. Wang, H. L. Zhang, L. P. Huang, G. Yu, *Nano Lett.* **2009**, *9*, 1752 – 1758.

[15] a) Y. Goto, K. Taniguchi, T. Omata, S. Otsuka-Yao-Matsuo, N. Ohashi, S. Ueda, H. Yoshikawa, Y. Yamashita, H. Oohashi, K. Kobayashi, *Chem. Mater.* **2008**, *20*, 4156 – 4160; b) G. J. Kovács, I. Bertóti, G. Radnóczi, *Thin Solid Films* **2008**, *516*, 7942 – 7946.

[16] Y. Koltypin, A. Fernandez, T. C. Rojas, J. Campora, P. Palma, R. Prozorov, A. Gedanken, *Chem. Mater.* **1999**, *11*, 1331 – 1335.

[17] Y. G. Li, H. L. Wang, L. M. Xie, Y. Y. Liang, G. S. Hong, H. J. Dai, *J. Am. Chem. Soc.* **2011**, *133*, 7296 – 7299.

[18] J. Xie, H. Zhang, S. Li, R. Wang, X. Sun, M. Zhou, J. Zhou, X. W. Lou, Y. Xie, *Adv. Mater.* **2013**, *25*, 5807 – 5813.

[19] D. Voiry, H. Yamaguchi, J. W. Li, R. Silva, D. C. B. Alves, T. Fujita, M. W. Chen, T. Asefa, V. B. Shenoy, G. Eda, M. Chhowalla, *Nat. Mater.* **2013**, *12*, 850 – 855.

[20] Y. F. Xu, M. R. Gao, Y. R. Zheng, J. Jiang, S. H. Yu, *Angew. Chem. Int. Ed.* **2013**, *52*, 8546 – 8550; *Angew. Chem.* **2013**, *125*, 8708 – 8712.

[21] J. Kibsgaard, Z. B. Chen, B. N. Reinecke, T. F. Jaramillo, *Nat. Mater.* **2012**, *11*, 963 – 969.

[22] a) J. K. Nørskov, T. Bligaard, J. Rossmeisl, C. H. Christensen, *Nat. Chem.* **2009**, *1*, 37 – 46; b) J. K. Nørskov, T. Bligaard, A. Logadottir, J. R. Kitchin, J. G. Chen, S. Pandelov, J. K. Norskov, *J. Electrochem. Soc.* **2005**, *152*, J23 – J26; c) J. Greeley, T. F. Jaramillo, J. Bonde, I. Chorkendorff, J. K. Norskov, *Nat. Mater.* **2006**, *5*, 909 – 913.

[23] X. F. Yang, A. Q. Wang, B. T. Qiao, J. Li, J. Y. Liu, T. Zhang, *Acc. Chem. Res.* **2013**, *46*, 1740 – 1748.

Received: August 18, 2015
Revised: September 12, 2015
Published online: October 16, 2015

